applied sciences

MDPI

Article

Electrochemical Removal of Cesium Ions via Capacitive Deionization Using an Ion-Exchange Layer Coated on a Carbon Electrode

Sang-Hun Lee [1,2], Mansoo Choi [2], Jei-Kwon Moon [2], Songbok Lee [2], Jihoon Choi [1] and Seonbyeong Kim [2,*]

[1] Department of Materials Science and Engineering, Chungnam National University, Daejeon 32134, Korea; leesh24@kaeri.re.kr (S.-H.L.); jihoonc@cnu.ac.kr (J.C.)
[2] Decommissioning Technology Research Division, Korea Atomic Energy Research Institute, Daejeon 34057, Korea; teracms@kaeri.re.kr (M.C.); njkmoon@kaeri.re.kr (J.-K.M.); songboklee@kaeri.re.kr (S.L.)
* Correspondence: sbkim@kaeri.re.kr; Tel.: +82-42-868-4681

Abstract: This study was conducted to evaluate the feasibility of using electrosorption to remove cesium (Cs^+) ions from aqueous solutions using the membrane capacitive deionization (MCDI) process. The electrochemical properties were analyzed using cyclic voltammetry (CV) and impedance spectroscopy (EIS). The activated carbon electrode coated by a polymer layer showed higher specific adsorption capacity (SAC) and removal efficiency of Cs^+ than the AC electrode. The effects of potential, flow rate, initial Cs^+ concentration, and pH values were investigated to optimize the electrosorption performance. The electrosorption capacity increased with an increase in the applied potential and the concentration of Cs^+ in the influent water. The pH value is an important parameter on electrosorption performance. The removal of Cs^+ ions was affected by the pH of the influent water because H^+ ions acted as competing ions during the electrosorption process. Cs^+ was preferentially adsorbed to the electrode in the early stages of adsorption but was later replaced by H^+. A higher presence of H^+ ions could reduce the adsorption capacity of Cs^+ ions. The ion-exchange layer coated AC electrode was shown to be favorable for the removal of Cs^+, despite the limited electrosorption ability in a highly acidic solution.

Keywords: capacitive deionization; electrosorption; Cs^+ ion removal; ion-exchange layer

check for updates

Citation: Lee, S.-H.; Choi, M.; Moon, J.-K.; Lee, S.; Choi, J.; Kim, S. Electrochemical Removal of Cesium Ions via Capacitive Deionization Using an Ion-Exchange Layer Coated on a Carbon Electrode. *Appl. Sci.* **2021**, *11*, 10042. https://doi.org/10.3390/app112110042

Academic Editor: Jorge Rodríguez-Chueca

Received: 8 October 2021
Accepted: 22 October 2021
Published: 27 October 2021

Publisher's Note: MDPI stays neutral with regard to jurisdictional claims in published maps and institutional affiliations.

Copyright: © 2021 by the authors. Licensee MDPI, Basel, Switzerland. This article is an open access article distributed under the terms and conditions of the Creative Commons Attribution (CC BY) license (https://creativecommons.org/licenses/by/4.0/).

1. Introduction

Nuclear energy provides a more steady and efficient supply of powerful energy than traditional energy. However, a large amount of radioactive waste is generated in nuclear power plants during their daily operations, maintenance, and decommissioning. In 2011, the nuclear power plant accident in Fukushima Daiichi, Japan, released large amounts of radioactive elements into the atmosphere, causing serious damage to the environment. Among the several nuclides, cesium ($^{137}Cs^+$) is one of the most dangerous radioactive elements. This material has a comparatively long half-life of 30 years and emits high-energy gamma radiation during the decay process [1]. Cs^+ is chemically similar to sodium and potassium. It can easily enter the human body and may induce severe diseases, such as cancer [2,3]. In addition, it can be dispersed in a variety of environments and integrate easily into soil and water, destroying eco-systems [4,5]. Therefore, effective techniques that remove Cs^+ are essential for solving these problems and sustaining the development of nuclear power plants.

Various technologies, including chemical precipitation, adsorption, membrane separation, and solvent extraction, have been widely studied for the removal of Cs^+ from wastewater [6–9]. However, these methods use excessive amounts of chemicals or consume high amounts of energy. Meanwhile, electrochemical methods have been developed and used as alternative options for the remediation of water and wastewater because of a

relatively simple process, ease of deposition on a large area, and the potential to serve as a low-cost commercial process that minimizes the generation of secondary radioactive waste. Moreover, the adsorption/desorption of ions can be easily controlled by the electrochemical method.

Among the electrochemical methods, capacitive deionization (CDI) is reportedly one of the most promising electrochemical methods for removing ions from aqueous solutions [10–15]. CDI is also an environmentally friendly process because it does not produce any additional contaminants during the operation. In the CDI process, the charged ions from the feed solution are adsorbed onto the electrical double layer (EDL) formed on the electrode surface [16,17]. CDI performance depends on the applied potential, flow rate, concentration of feed solution, and electrode material.

The CDI process has been extensively applied for many types of ions, including Na^+, NH^{4+}, Cu^{2+}, Zn^{2+}, Cl^-, F^-, and NO^{3-} [18–21]. CDI can also be used to remove radionuclides from contaminated wastewater from nuclear power plants prior to release. Recently, it was reported that the activated carbon cloth (ACC)-based CDI electrode exhibited the Sr^{2+} removal efficiency of 41.45% for an applied potential of 1.2 V [22]. In another study, the CDI process was used for the removal of Co^{2+} and Cs^+ from aqueous solutions. The ACC-based CDI electrode achieved the maximum adsorption capacity of Co^{2+} and Cs^+, which was 16.7 mg g^{-1} and 22.9 mg g^{-1} at 1.2 V and 20 mg L^{-1}, respectively [23]. It is necessary to study the electrosorption performance under various experimental conditions, particularly the removal of Cs^+ under acidic solutions, Huysken et al. [24] investigated electrosorption in influent with a pH of 2.6 and reported that H^+ derived from acetic acid competed for Na^+ during the electrosorption process. In addition, Shen et al. [25] reported that when H^+ ions are present in higher concentrations than In^{3+} ions, H^+ ions are preferentially adsorbed to the electrode in the early stage of charging. Thus, it is important to understand the fluctuating performance according to operating conditions in aqueous solutions for the removal of Cs^+ during the CDI process.

Modification of CDI can be achieved by inserting an ion-exchange membrane (IEM) over the electrodes to enhance the properties of the system. This improves the ion removal performance and life cycle of the electrodes. An important advantage of membrane capacitive deionization (MCDI) compared to conventional CDI is the ion exchange membrane, which impedes the adsorption of counter ions while preventing co-ions from leaving the electrode region [26]. In this context, MCDI achieves better deionization rates than typical CDI in wastewater treatment with higher charge efficiency [27,28].

This study evaluated the electrosorptive removal performance of Cs^+ from aqueous solutions using the MCDI process. Cyclic voltammetry (CV), impedance spectroscopy (EIS) and surface characterization were conducted to elucidate the interaction between Cs^+ ions and the electrode surface. The MCDI process was compared to the conventional CDI process for the removal of Cs+ from aqueous solutions. This system was operated in a single-pass mode to investigate the electrosorption performance for Cs^+. To optimize the removal performance of Cs^+, the effects of potential, flow rate, initial Cs^+ concentration, and pH value were investigated. We also discussed the electrosorption selectivity between Cs^+ and H^+. This study demonstrates the promising potential for using the CDI method as a means of removing Cs^+ ions in acid-based aqueous solutions.

2. Materials and Methods

2.1. Preparation of a Carbon Electrode

The commercial activated carbon (AC) electrodes and AC electrodes coated with cation and anion exchange polymers were obtained from Sion Tech Co., Seoul, Korea. The carbon electrodes consisted of a carbon slurry containing activated carbon P-60 (Kuraray Chemical Co., Kurashiki, Japan) on a graphite sheet as a current collector. The physical properties of the AC are shown in Table 1. The size of electrodes was 100 mm × 100 mm.

Table 1. Physical properties of activated carbon powder.

Type	Sample	S_{BET} (m^2 g^{-1})	V_{total} (cm^3 g^{-1})	d_{BJH} (nm)
Powder	Activated carbon	1250.27	0.55	1.77

2.2. Electrochemical Property of a Carbon Electrode

The morphology of the electrodes was analyzed with a field emission scanning electron microscope (FE-SEM, Thermoscientific Cios2). The specific surface area and pore volume were measured by Brunauer-Emmett-Teller (BET) and Barrett-Joyner-Halenda (BJH) methods using N_2 adsorption-desorption isotherms at −196 °C, respectively (Trista II 3020). For this analysis, the samples were degassed at 120 °C overnight before the measurements.

To evaluate the electrochemical performance of the electrodes, cyclic voltammetry (CV) and electrical impedance spectroscopy (EIS) measurements were carried out in a 0.5 M $CsNO_3$ solution using a three-electrode system. A platinum rod and saturated Ag/AgCl (3 M KCl) electrodes were used as counter and reference electrodes, respectively. Both CV and EIS were obtained with ZIVE MP2 (WonA tech Co., Daejeon, Korea). CV measurement of the electrode was performed in the potential range from −0.7 to 0.7 (vs. Ag/AgCl) at a 2 mV s^{-1} potential scan rate. The impedance spectra were obtained in the frequency range from 100 kHz to 20 mHz with an amplitude of 10 mV.

2.3. Capacitive Deionization Experiment

The MCDI unit cell consisted of two parallel carbon electrodes. To prevent short-circuiting, a spacer with a thickness of 100 μm (100 mesh, Nylon) was used to separate each pair of electrodes. In addition, the spacer was used as a flow channel for the influent water within the MCDI cell. The schematic of the single-pass MCDI experiment and cell configuration is depicted in Figure 1. The influent water flowed in from the marginality of the electrode and flowed out from the center of the electrode. A unit cell was assembled by placing plexiglas on both sides of the electrodes.

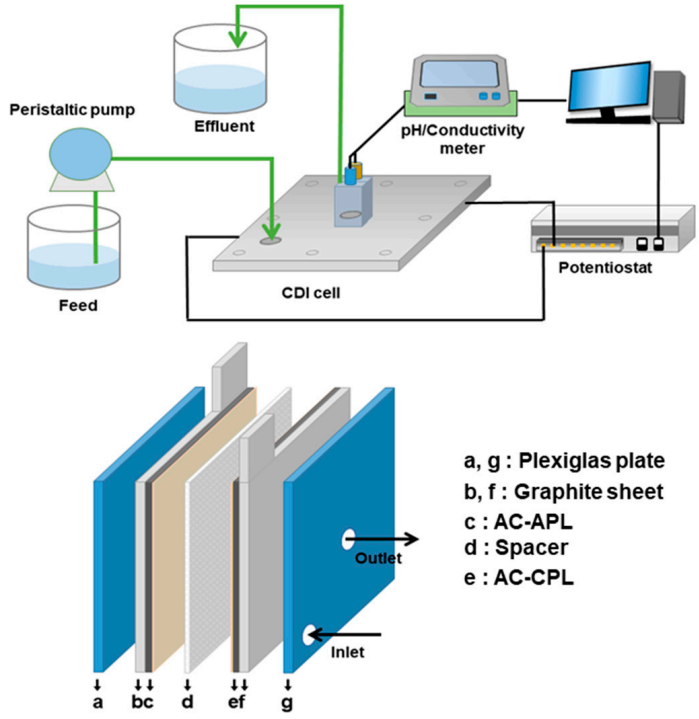

Figure 1. Schematic diagram of the MCDI experiment and cell configuration.

Deionization experiments were performed by the single-pass method, where the influent was passed through the MCDI cell. The concentration, pH, and flow rate of the feed solution varied from 50~200 mg L^{-1} to 2~4 and 10~30 mL min^{-1}, respectively. An adsorption experiment was conducted at different cell potentials (0.8, 1.0, 1.2, 1.4 V) through a potentiostat (WPG100, WonA tech Co., Seoul, Korea). A desorption test was conducted by changing the cell potential to 0 V immediately after the adsorption test. At each cell potential, the adsorption/desorption experiment was repeated three times in succession to ensure equilibrium. A conductivity and pH measurement system (Orion Versa Star Pro, Thermo Fisher Scientific, Waltham, MA, USA) was installed at the outlet of the cell and continuously monitored at intervals of 5 s. The concentration of Cs^+ ions was measured using inductively coupled plasma optical emission spectroscopy (ICP-OES, Perkin Elmer, Midland, ON, Canada).

The specific adsorption capacity (SAC) of the electrode was calculated using the following equation:

$$\mathrm{SAC(mg/g)} = \frac{V(C_0 - C_{avg})}{m} \quad (1)$$

where V is the total volume of influent water supplied to the cell during the adsorption process; C_0 and C_{avg} are the initial influent concentration and average effluent concentration, respectively; and m is the mass of the carbon electrode. The specific adsorption rate (SAR) was obtained by dividing the SAC value with the adsorption time.

The charge efficiency (Λ) is the ratio of the salt adsorption amounts over the charge in a CDI, which was calculated by the following equation:

$$\Lambda = \frac{V \cdot F \cdot (C_0 - C_{avg})}{M_w \int I dt} \quad (2)$$

where F is Faraday's constant, M_w is the molar mass of $CsNO_3$, and I is the current density.

The removal efficiency was calculated by the following equation:

$$\text{Removal efficiency } (\%) = \frac{(C_0 - C_{avg})}{C_0} \times 100 \quad (3)$$

3. Results and Discussion

3.1. Charaterization of the Electrodes

A large surface area and suitable pore volume of porous carbon are key factors for high electrosorption performance in the CDI process. Figure 2 shows the SEM images of the surface of the activated carbon (AC) electrode and the activated carbon electrode coated by the cation polymer layer, referred to as the AC-CPL. The AC electrode was porous and rough, whereas the AC-CPL had a relatively uniform and smooth surface owing to the influence of a cation exchange layer. Figure 2c shows that the surface of the carbon electrode was completely covered with a cation-exchange layer that had a maximum thickness of about 3.4 μm. The shape of the sturdy electrode surface was expected to mitigate the degradation of electrode performance caused by the physical adsorption of wastewater-related contaminants since there is less opportunity to come into contact with contaminants and adsorb them [12].

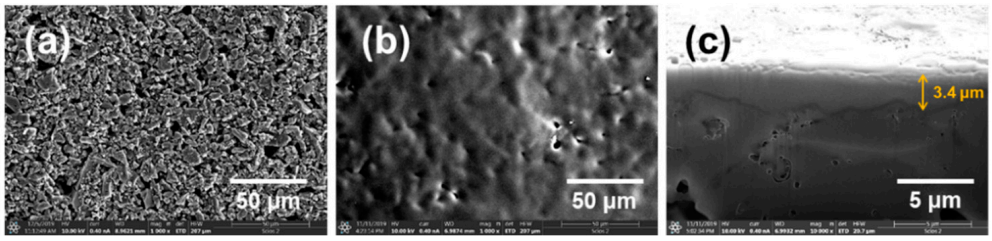

Figure 2. SEM image of surface of activated carbon electrode (**a**); SEM images of surface (**b**) and cross-section (**c**) of the activated carbon electrode coated by the cation polymer layer.

3.2. Electrochemical Charaterization of the Electrodes

Cyclic voltammetry (CV) was performed to characterize the electrochemical properties of both electrodes. Figure 3 shows the CV curves of the AC and the AC-CPL at a scan rate of 2 mV s^{-1} in the voltage range of −0.7 to 0.7 V. The CV curve for the AC represents typical capacitor behavior and has a nearly rectangular shape. In contrast to the symmetrical AC, the curve for AC-CPL has a relatively high current value at the whole potential. Additionally, anodic and cathodic peaks were observed at ~0.20 and −0.52 V, respectively, which corresponds to the Faradaic reactions provided by the surface functionalities of the cation-exchange layer. The specific capacitance of the AC-CPL calculated from the CV result was 113.94 F g^{-1}, which had an increased value compared with that of the AC (73.67 F g^{-1}). The presence of the cation-exchange layer contributed to improving the capacitance of the carbon electrode.

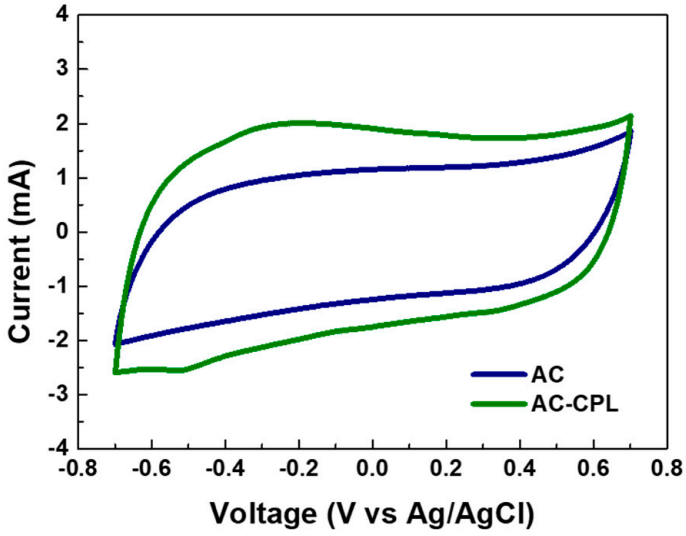

Figure 3. Comparison of cyclic voltammetry curves of AC and AC-CPL in 0.5 M $CsNO_3$ at 2 mV s^{-1} scan rate.

Electrochemical impedance spectroscopy (EIS) analysis was carried out to investigate the electrical resistance of the electrode materials. Figure 4 shows the Nyquist plots of the alternating current (AC) impedance spectroscopy for the prepared electrodes. The intercept of the curve at the real axis (Z′) in the high-frequency range corresponds to the solution resistance (R_s). The diameter of the semicircle represents the charge-transfer resistance (R_{ct}), also known as the interfacial reaction resistance. The linear part of the low-frequency region represents the Warburg impedance corresponding to the frequency dependence of ion diffusion/transport in aqueous solution [29]. The R_s values were measured at 7.8 ohms and 9.0 ohms for the AC and AC-CPL, respectively. The R_{ct} associated with the electrode-electrolyte interface was determined from the width of the semicircle that appears at high frequencies. The R_{ct} was lower in the AC-CPL than in the AC, which might be related to the pseudo-capacitive contribution increased by the cation-exchange layer. The thin and

firmly coated cation-exchange layer played a positive role in reducing the charge resistance of the AC.

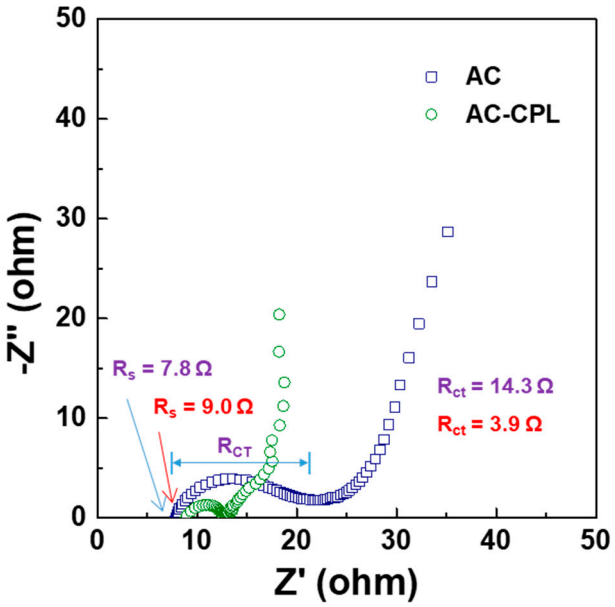

Figure 4. Nyquist plots of AC, and AC-CPL in 0.5 M $CsNO_3$ solution. (Color of navy: R_s and R_{ct} of the AC, color of olive: R_s and R_{ct} of the AC-CPL).

3.3. CDI Performance of the Electrodes

Figure 5 shows the flow rate dependence on the SAC and the removal efficiency for the AC and AC-CPL. The SAC value showed a tendency to decrease for the AC as the flow rate increased but showed a progressively increased value for the AC-CPL electrode at the same flow rate. The SAC values were higher for the AC-CPL than for the AC. In the AC electrode, the SAC value showed a tendency to decrease with a flow rate increase because the electrosorption process requires high contact time between the electrode surface and the ionic solution. The highest removal efficiency of Cs^+ was 5 mL min^{-1} for the AC and 10 mL min^{-1} for the AC-CPL. Then the efficiency gradually decreased as the flow rate increased because a low flow rate provided sufficient contact time for reactants with the electrode.

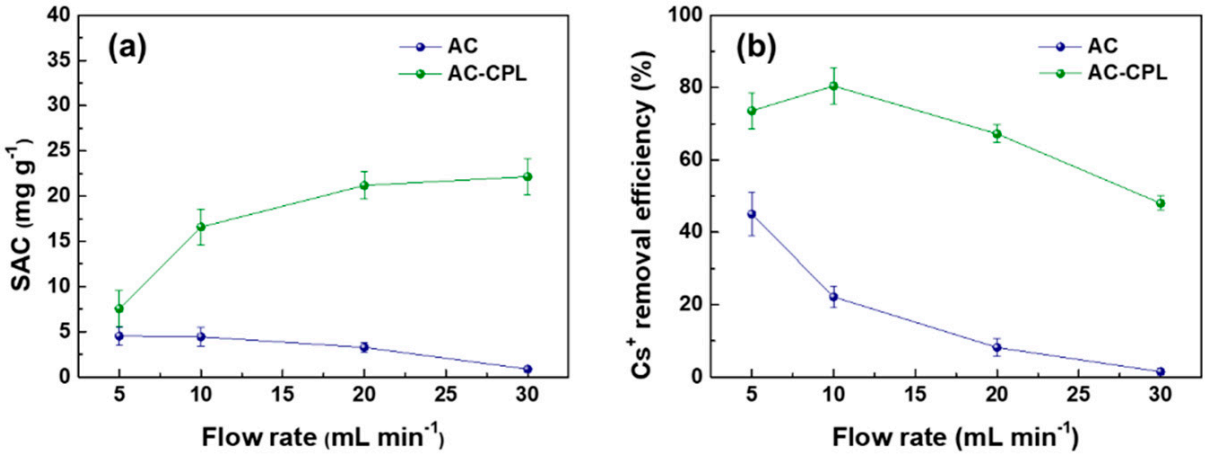

Figure 5. Comparison of the AC, and the AC-CPL for (**a**) specific adsorption capacity of Cs^+ ions and (**b**) removal efficiency according to the flow rate (Experimental conditions: Influent of 200 mg L^{-1} Cs^+ ions at pH 3 solution was fed at 1.2 V for 10 min).

Figure 6a shows the conductivity of the effluent for the AC-CPL according to the potential variation from 0.8 V to 1.4 V. The tests were conducted by maintaining a constant flow rate at 20 mL min^{-1} for 10 min. As soon as an electric potential was applied, the conductivity decreased sharply. The reason for the decreased electrical conductivity at the initial stage was due to the accumulation of charged ions by the electrodes. Following this, the electrical conductivity of the effluent water increased. The higher applied potential induced a stronger electrostatic force, which had a positive effect on the electrosorption performance. [17] A desorption potential of 0 V was applied immediately after adsorption. The conductivity increased rapidly, and the value close to the concentration of the injected water was measured. The results revealed that desorption proceeded rapidly, and the regeneration of the electrode in the CDI system was facile. The specific adsorption capacity and charge efficiency of Cs^+ according to the applied potential are depicted in Figure 6b. The SAC value increased with increasing applied potential, indicating that the electrosorption performance was enhanced. The charging efficiency showed the highest value at 1.2 V. Charge efficiency can be defined as the ratio of the adsorbed amount of salt over the charge, and is an important parameter in evaluating electrosorption performance in CDI cells. The energy requirement per ion removed can be explained in terms of the value of the charge efficiency, and the higher the charge efficiency, the lower the energy consumption. In general, the charge efficiency depends on the cell potential, which increases as the charging potential increases [30]. The applied potential at 1.4 V reduced the charge efficiency, which is reportedly due to the possibility of side reactions (e.g., water electrolysis, oxidation of carbon electrode) [31–33]. Thus, the applied potential of 1.2 V was used in the follow-up test.

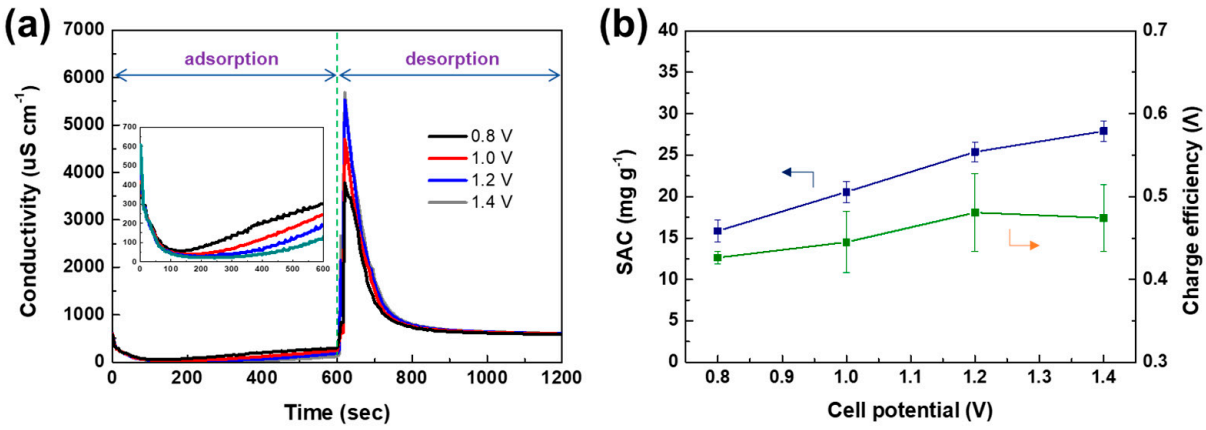

Figure 6. (**a**) Effluent conductivity of $CsNO_3$ according to the cell potentials during the adsorption process and (**b**) specific adsorption capacity of Cs^+ ions and charge efficiency (Experimental conditions: Influent of 200 mg L^{-1} Cs^+ ions at pH 3 solution was fed with a flow rate of 20 mL min^{-1} for 10 min adsorption/desorption, respectively).

Figure 7 shows the maximum adsorption capacity of the AC-CPL depending on the concentration of Cs^+ and the flow rate of the influent water. As shown in Figure 7, the maximum adsorption capacity increased according to the Cs^+ concentration in the influent water regardless of the flow rate. These results can be explained by Gouy-Chapman-Stern (GCS) theory and electric double layer expansion [34]. An electric double layer can be more effectively formed on the porous structure of the carbon electrode, along with an increase in the ion concentration of the solution, thereby providing more advantageous conditions for the electrosorption process. When the Cs^+ ion concentration in the influent water was 50 mg L^{-1} and 100 mg L^{-1}, the maximum adsorption capacity decreased according to an increase in the flow rate, whereas the maximum adsorption capacity increased according to an increase in the flow rate in the influent water of 200 mg L^{-1} Cs^+. The enhanced adsorption capacity of 200 mg L^{-1} Cs^+ influent water is attributed to fast ion transport [35].

The fast flow rate, especially at high concentrations of influent, demonstrates excellent rate capability along with a high ion adsorption capacity.

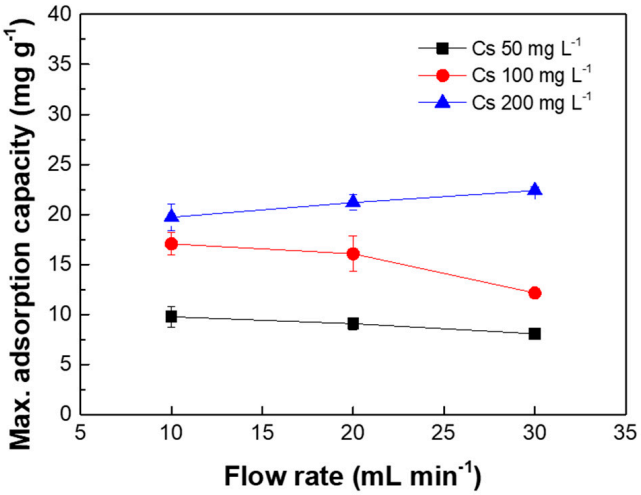

Figure 7. Maximum adsorption capacity of Cs^+ ions as a function of flow rate and influent concentration. Adsorption was conducted until the cell potential reached 1.2 V (Experimental conditions: Influent of pH 3 was fed for 60 min adsorption).

The radioactive wastewater containing Cs^+ generated in nuclear facilities is stored in a highly acidic solution, and the pH value is an important indicator. We measured the effect of pH to further investigate the electrosorption performance for the AC-CPL. Figure 8a shows the concentration of Cs^+ in the effluent water during the electrosorption process. The concentration of Cs^+ in the effluent decreased rapidly at the initial stage and gradually increased to the initial concentration. In particular, the amount of adsorbed Cs^+ decreased after the electrode reached saturation at pH 3, which was presumably due to the co-ions release from the EDL near the pores and neutral salt discharge from the electrode [12]. We monitored the pH variation of the influent solution during the electrosorption process, and the results are shown in Figure 8b. In contrast to the concentration curves of Cs^+ ions in the effluent, the water pH variation showed the opposite trend, indicating that H^+ ions were competitively electrosorbed at the electrode surface. This result was definitively observed at pH 2 (Figure S1). It shows that the concentration of the effluent reached 31.92 mg L^{-1} in the first 45 s and increased rapidly to the initial influent concentration. The maximum adsorption capacity was 0.75 mg g^{-1}, and it can be seen that the adsorption of H^+ dominated through the results of the pH profile. Generally, the pH of the influent water directly affects the zeta potentials by adsorbing H^+ or OH^- ions on the surface of electrodes [36]. In acidic conditions, the zeta potential was shielded due to the adsorption of more H^+, and consequently, the electrosorption performance decreased significantly [13].

Ragone plots of SAR vs. SAC in the CDI system visually show the electrosorption performance of the electrode. As presented in Figure 9, the SAC increased, and the SAR decreased during the electrosorption process. The surface area adsorbed on the electrode reduced in size as the electrosorption proceeded. When the concentration of Cs^+ in the influent water increased, the Ragone plot shifted to the upper and righter area. The SAR and SAC show similar initial values, but as the adsorption time elapsed, most of the SAR values showed a decreasing curve, and the SAC value at pH 4 reached a constant value. At pH 3, the SAC value decreased as the adsorption time increased, which was largely due to the adsorption of H^+ competing ions, as mentioned in Figure 8.

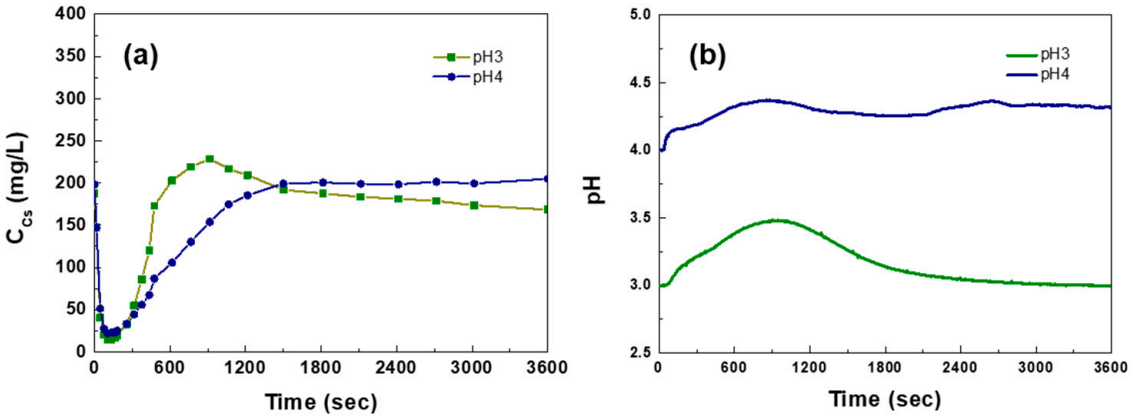

Figure 8. Changes in Cs^+ concentration (**a**), and pH of effluent (**b**) according to pH in the influent (Experimental conditions: Influent of 200 mg L^{-1} Cs^+ ions concentration was fed with a flow rate of 20 mL min^{-1} at 1.2 V for 60 min adsorption).

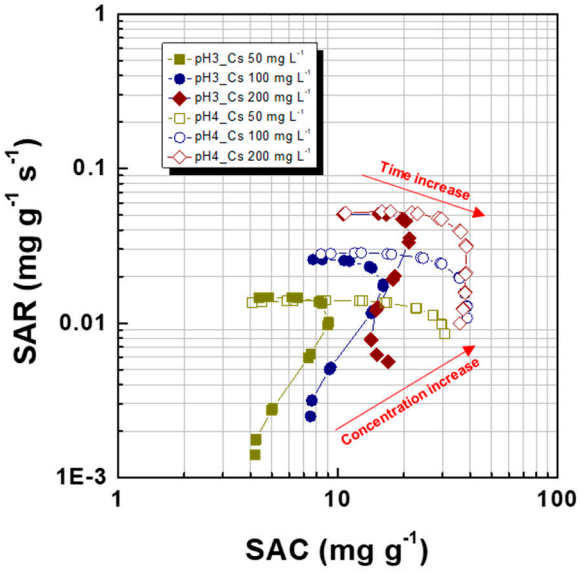

Figure 9. Ragone plots of effluent according to the concentration and pH of Cs^+ ions in the influent (Experimental conditions: Influent of pH 3 or pH 4 was fed with a flow rate of 20 mL min^{-1}).

4. Conclusions

In this study, we investigated the parameters for the effective removal of Cs^+ ions from an aqueous solution using an AC-CPL by a CDI process. The CEL-AC electrode confirmed higher SAC and removal efficiency for Cs^+ ions than the AC electrode. The ion adsorption capacity of the AC-CPL was strongly dependent on the applied potential, flow rate, initial concentration of Cs^+, and initial pH value. When the potential increased, the adsorption capacity increased, and the charge efficiency decreased at 1.4 V. The maximum adsorption capacity decreased with increasing flow rate in 50 and 100 mg L^{-1} Cs^+ influent water, respectively. On the other hand, the maximum adsorption capacity increased with the increase of the flow rate in 200 mg L^{-1} Cs^+ influent water. The effect of pH on the electrosorptive removal of Cs^+ ions was examined and showed that Cs^+ ions were preferentially adsorbed to the electrode in the early stage of adsorption. However, the adsorbed Cs^+ ions were gradually replaced by H^+ ions, especially in the case of low pH. A greater presence of H^+ ions reduced the adsorption capacity of the Cs^+ ions. These findings indicate that, with the exception of highly acidic solutions, the electrosorptive removal method using an AC-CPL can be applied successfully for the removal of Cs^+ ions from acidic waste-water solutions.

Supplementary Materials: The following are available online at https://www.mdpi.com/article/10.3390/app112110042/s1, Figure S1: Changes in concentration and pH of Cs^+ ions of effluent during the adsorption process (Experimental conditions: Influent of 50 mg L^{-1} Cs^+ ions at pH 2 was fed with a flow rate of 20 mL min^{-1} at 1.2 V for 60 min).

Author Contributions: Conceptualization, S.-H.L., M.C. and S.L.; methodology, S.-H.L., S.L. and J.-K.M.; validation, S.K.; formal analysis, S.-H.L.; investigation, S.-H.L. and S.L.; resources, S.K.; data curation, S.-H.L. and M.C.; writing—original draft preparation, S.-H.L. and M.C.; writing—review and editing, S.-H.L., M.C. and J.-K.M.; supervision, J.C. and J.-K.M.; project administration, J.-K.M. and S.K. All authors have read and agreed to the published version of the manuscript.

Funding: This research received no external funding.

Institutional Review Board Statement: Not applicable.

Informed Consent Statement: Not applicable.

Data Availability Statement: The data presented in this study are available on request from the corresponding author.

Acknowledgments: This research was supported by the National Research Foundation of Korea (NRF) grant funded by the Korean government, Ministry of Science and ICT (No. 2017M28A5015144).

Conflicts of Interest: The authors declare no conflict of interest.

References

1. Yoshihara, T.; Matsumura, H.; Hashida, S.; Nagaoka, T. Radiocesium contaminations of 20 wood species and corresponding gamma-ray rates around the canopies at 5 months after the Fukushima nuclear power plant accident. *J. Envrion. Radioact.* **2013**, *115*, 60–68. [CrossRef]
2. Castrillejo, M.; Casacuberta, N.; Breier, C.F.; Pike, S.M.; Masque, P.; Buesseler, K.O. Reassessment of ^{90}Sr, ^{137}Cs, and ^{134}Cs in the coast off Japan derived from the Fukushima Dai-Ichi nuclear accident. *Environ. Sci. Technol.* **2016**, *50*, 173–180. [CrossRef] [PubMed]
3. Hoeve, J.E.T.; Jacobson, M.Z. Worldwide health effects of the Fukushima Daiichi nuclear accident. *Energy Environ. Sci.* **2012**, *5*, 8743–8757. [CrossRef]
4. Lee, C.P.; Kuo, Y.M.; Tsai, S.C.; Wei, Y.Y.; Teng, S.P.; Hsu, C.N. Numerical analysis for characterizing the sorption/desorption of cesium in crushed granite. *J. Radioanal. Nucl. Chem.* **2008**, *275*, 343. [CrossRef]
5. Kumamoto, Y.; Aoyama, M.; Hamajima, Y.; Murata, A.; Kawano, T. Impact of Fukushima-derived radiocesium in the western North Pacific Ocean about ten months after the Fukushima Dai-ichi nuclear power plant accident. *J. Environ. Radioact.* **2015**, *140*, 114–122. [CrossRef]
6. Avramenko, V.; Bratskaya, S.; Zheleznov, V.; Sheveleva, I.; Voitenko, O.; Sergienko, V. Colloid stable sorbents for cesium removal: Preparation and application of latex particles functionalized with transition metals ferrocyanides. *J. Hazard Mater.* **2011**, *186*, 1343–1350. [CrossRef] [PubMed]
7. Yang, H.M.; Park, C.W.; Kim, I.K.; Yoon, I.H. Hollow flower-like titanium ferrocyanide structure for the highly efficient removal of radioactive cesium form water. *Chem. Eng. J.* **2020**, *392*, 123713. [CrossRef]
8. Duhart, A.; Dozol, J.F.; Rouquette, H.; Deratani, A. Selective removal of cesium from model nuclear waste solutions using a solid membrane composed of an unsymmetrical calix[4] arenebiscrown-6 bonded to an immobilized polysiloxane backbone. *J. Membr. Sci.* **2001**, *185*, 145–155. [CrossRef]
9. Delchet, C.; Tokarev, A.; Dumail, X.; Toquer, G.; Barre, Y.; Guari, Y.; Guerin, C.; Larionova, J.; Grandjean, A. Extraction of radioactive cesium using innovative functionalized porous materials. *RSC Adv.* **2012**, *2*, 5707–5716. [CrossRef]
10. Lee, B.; Park, N.; Kang, K.S.; Ryu, H.J.; Hong, S.H. Enhanced capacitive deionization by dispersion of CNTs in activated carbon electrode. *ACS Sustain. Chem. Eng.* **2018**, *6*, 1572–1579. [CrossRef]
11. Porada, S.; Zhao, R.; van der Wal, A.; Presser, V.; Biesheuvel, P.M. Review on the science and technology of water deslination by capacitive deionization. *Prog. Mater. Sci.* **2013**, *58*, 1388–1442. [CrossRef]
12. Kim, D.I.; Dorji, P.; Gwak, G.; Phuntsho, S.; Hong, S.; Shon, H. Reuse of municipal wastewater via membrane capacitive deionization using ion-selective polymer-coated carbon electrodes in pilot-scale. *Chem. Eng. J.* **2019**, *372*, 241–250. [CrossRef]
13. Choi, J.; Lee, H.; Hong, S. Capacitive deionization (CDI) integrated with monovalent cation selective membrane for producing divalent cation-rich solution. *Desalination* **2016**, *400*, 38–46. [CrossRef]
14. Mossad, M.; Zou, L. A study of the capacitive deionization performance under various operational conditions. *J. Hazard Mater.* **2012**, *213*, 491–497. [CrossRef]
15. Pastushok, O.; Zhao, F.; Ramasamy, D.L.; Sillanpää, M. Nitrate removal and recovery by capacitive deionization (CDI). *Chem. Eng. J.* **2019**, *375*, 121943. [CrossRef]
16. Park, K.K.; Lee, J.B.; Park, P.Y.; Yoon, S.W.; Moon, J.S.; Eum, H.M.; Lee, C.W. Development of a carbon sheet electrode for electrosorption desalination. *Desalination* **2007**, *206*, 86–91. [CrossRef]

17. Welgemoed, T.J.; Schutte, C.F. Capacitive Deionization Technology^{TM}: An alternative desalination solution. *Desalination* **2005**, *183*, 327–340. [CrossRef]
18. Tang, W.; Kovalsky, P.; He, D.; Waite, T.D. Fluoride and nitrate removal from brackish groundwaters by batch-mode capacitive deionization. *Water Res.* **2015**, *84*, 342–349. [CrossRef] [PubMed]
19. Laxman, K.; Myint, M.T.Z.; Al-Abri, M.; Sathe, P.; Dobretsov, S.; Dutta, J. Desalination and disinfection of inland brackish ground water in a capacitive deionization cell using nanoporous activated carbon cloth electrodes. *Desalination* **2015**, *632*, 126–132. [CrossRef]
20. Wimalasiri, Y.; Mossad, M.; Zou, L. Thermodynamics and kinetics of adsorption of ammonium ions by graphene laminate electrodes in capacitive deionization. *Desalination* **2015**, *357*, 178–188. [CrossRef]
21. Oda, H.; Nakagawa, Y. Removal of ionic substances from dilute solution using activated carbon electrodes. *Carbon* **2003**, *41*, 1037–1047. [CrossRef]
22. Liu, X.J.; Wang, J.L. Electro-adsorption characteristics and mechanism of Sr^{2+} ions by capacitive deionization and CFD analysis study. *Prog. Nucl. Energy* **2021**, *133*, 103628. [CrossRef]
23. Liu, X.J.; Wang, J.L. Electro-assisted adsorption of Cs(I) and Co(II) from aqueous solution by capacitive deionization with activated carbon cloth/graphene oxide composite electrode. *Sci. Total Environ.* **2020**, *749*, 141524. [CrossRef] [PubMed]
24. Huyskens, C.; Helsen, J.; Groot, W.J.; de Haan, A.B. Membrane capacitive deionization for biomass hydrolysate desalination. *Sep. Purif. Technol.* **2013**, *118*, 33–39. [CrossRef]
25. Shen, Y.Y.; Wu, S.W.; Hou, C.H. Exploring the electrosorption selectivity and recovery of indium ions with capacitive deionization in acidic solution. *J. Colloid Interf. Sci.* **2021**, *586*, 819–829. [CrossRef]
26. Tang, W.; He, D.; Zhang, C.; Waite, T.D. Optimization of sulfate removal from brackish water by membrane capacitive deionization (MCDI). *Water Res.* **2017**, *121*, 302–310. [CrossRef] [PubMed]
27. Liang, P.; Yuan, L.; Yang, X.; Zhou, S.; Huang, X. Coupling ion-exchangers with inexpensive activated carbon fiber electrodes to enhance the performance of capacitive deionization cells for domestic wastewater desalination. *Water Res.* **2013**, *47*, 2523–2530. [CrossRef]
28. Jiang, J.; Kim, D.I.; Dorji, P.; Phuntsho, S.; Hong, S.; Shon, H.K. Phosphorus removal mechanisms from domestic wastewater by membrane capacitive deionization and system optimization for enhanced phosphate removal. *Process Saf. Environ.* **2019**, *126*, 44–52. [CrossRef]
29. Zhang, D.; Yan, T.; Shi, L.; Peng, Z.; Wen, X.; Zhang, J. Enhanced capacitive deionization performance of graphene/carbon nanotube composites. *J. Mater. Chem.* **2012**, *22*, 14696. [CrossRef]
30. Zhao, R.; Biesheuvel, P.M.; Miedema, H.; Bruning, H.; van der Wal, A. Charge Efficiency: A Functional Tool to Probe the Double-Layer Structure Inside of Porous Electrodes and Application in the Modeling of Capacitive Deionization. *J. Phys. Chem. Lett.* **2010**, *1*, 205–210. [CrossRef]
31. He, D.; Wong, C.E.; Tang, W.; Kovalsky, P.; Waite, T.D. Faradaic reactions in water desalination by batch-mode capacitive deionization. *Environ. Sci. Technol. Lett.* **2016**, *3*, 222–226. [CrossRef]
32. Kim, T.; Yu, J.; Kim, C.; Yoon, J. Hydrogen peroxide generation in flow-mode capacitive deionization. *J. Electroanal. Chem.* **2016**, *776*, 101–104. [CrossRef]
33. Shapira, B.; Avraham, E.; Aurbach, D. Side reactions in capacitive deionization (CDI) processes: The role of oxygen reduction. *Electrochim. Acta* **2016**, *220*, 285–295. [CrossRef]
34. Boo, H.; Park, S.; Ku, B.; Kim, Y.; Park, J.H.; Kim, H.C.; Chung, T.D. Ionic strength controlled virtual area of mesoporous platinum electrode. *J. Am. Chem. Soc.* **2004**, *126*, 4524–4525. [CrossRef] [PubMed]
35. Kim, N.; Lee, E.; Su, X.; Kim, C. Parametric investigation of the desalination performance in multichannel membrane capacitive deionization (MC-MCDI). *Desalination* **2021**, *503*, 114950. [CrossRef]
36. Skwarek, E.; Bolbukh, Y.; Tertykh, V.; Janusz, W. Electrokinetic properties of the pristine and oxidized MWCNT depending on the electrolyte type and concentration. *Nanoscale Res. Lett.* **2016**, *11*, 1–17. [CrossRef]